2016 IEEE/RSJ International Conference on Robotics and Automation (ICRA)
May 16-21, 2016, Stockholm, Sweden.

Soft pop-up mechanisms for micro surgical tools: design and characterization of compliant millimeter-scale articulated structures

S. Russo[1+], T. Ranzani[1+], J. Gafford[1], C.J. Walsh[2], R.J. Wood[2]

***Abstract*— This paper introduces a manufacturing technique which enables the integration of soft materials and soft fluidic micro-actuators in the Pop-up book MEMS paradigm. Such a technique represents a promising approach to the design and fabrication of low cost and scalable articulated mechanisms provided with sensing capabilities and on-board actuation with potential applications in the field of minimally invasive surgery. Design and integration of soft components in the rigid-flex laminates is described along with the resulting soft pop-up mechanisms realized at different scales. Prototype characterization is presented, demonstrating forces and dexterity in a range suitable for surgical applications, as well as the possibility to integrate sensing capabilities. Based on these results, a multi-articulated robotic arm is fabricated and mounted on top of an endoscope model to provide a proof of concept of simple robotic mechanisms that could be useful in a surgical scenario.**

I. INTRODUCTION

The drive towards early detection of cancer and minimally invasive surgery (MIS) motivates the research in the development of miniaturized smart instruments to perform treatment with minimal access trauma [1]. The fabrication of articulated structures, able to effectively perform tasks in complex and highly unstructured environments such as the human body, presents several challenges mainly due to the lack of viable manufacturing techniques and actuation strategies at these scales. Instruments need to provide the surgeon with sensory feedback as well as dexterity and forces necessary at the surgical site, especially when flexible endoscopes are used to reach the target area such as in natural orifice transluminal endoscopic surgery (NOTES) [2]. Several robotic systems [3] as well flexible endoscopic multi-task platforms [4] have been proposed to overcome limitations of current instruments and provide better and more sophisticated devices to surgeons. However, when dealing with endoscopic procedures, current devices still suffer from limited maneuverability, manipulation capabilities and do not integrate sensing, which limit the possibility to perform advanced endoluminal surgery [3]. Additional solutions consist of integrating robotic arms or manipulation aids directly on the tip of an endoscope [5][6][7].

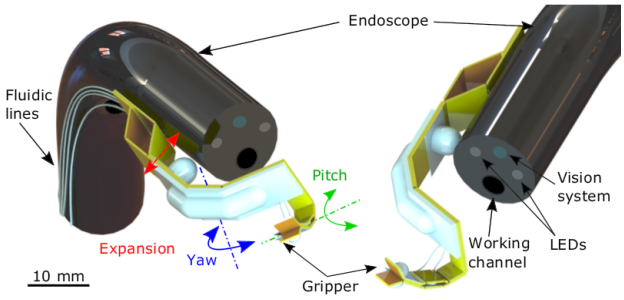

Fig. 1. CAD rendering of combined soft pop-up mechanisms that build an articulated mechanism at the tip of an endoscope to provide additional dexterity and manipulation capabilities during endoscopic procedures.

This strategy allows increasing dexterity and instrument triangulation (deflecting the instruments from the vision system), without losing flexibility of the endoscope in reaching the target. However, these solutions introduce technical challenges: proximal actuation requires cables along the endoscope, resulting in cable friction and backlash which can affect accuracy, controllability and thus intuitiveness of the system [3][8]. Distal actuation approaches still lack viable technologies due to challenges for scalability and safety of the materials, currents and voltages needed [9]. A promising approach has been proposed by Webster et al. where active cannulas are used in combination with conventional endoscopes for transurethral prostate surgery [10] and transoral lung surgery [11]. Recent studies have focused on increasing the amount of articulation achievable at the instrument tip, [11] as well as integrating sensing capabilities [12] for these systems. The Pop-up book MEMS manufacturing paradigm creates three dimensional microstructures and devices, based on the folding of multilayer rigid-flex laminates [13]. This method enables fabrication of highly complex structures with embedded actuation and sensing and it has been successfully applied in fabricating functional bioinspired robots [14] as well as mechanisms and sensors for surgical applications [15][16][17]. Advantages of this approach include batch manufacturing (low cost) and flexibility in the material selection [13]. In order to develop an articulated robotic arm with on-board actuation and sensing, we need to consider different actuation strategies as well as material combinations to provide safe interaction with the biological structures, matching the impedance of the environment. Soft technologies have been recently proposed for medical devices [18], [19]. Soft micro actuators for medical applications have also

+The authors equally contributed to this work

*The authors gratefully acknowledge support from DARPA (award # FA8650-15-C-7548) and the Wyss Institute for Biologically Inspired Engineering.

[1]S. Russo, T. Ranzani (corresponding author), J. Gafford are with the John A. Paulson School of Engineering and Applied Sciences at Harvard University, Cambridge MA 02138, USA srusso,tranzani, jgafford@seas.harvard.edu

[2]R. Wood and C. Walsh are with the John A. Paulson School of Engineering and Applied Sciences at Harvard University, Cambridge MA 02138, USA, and also with the Wyss Institute for Biologically-Inspired Engineering, Boston, MA 02115, USA rjwood, walsh@seas.harvard.edu

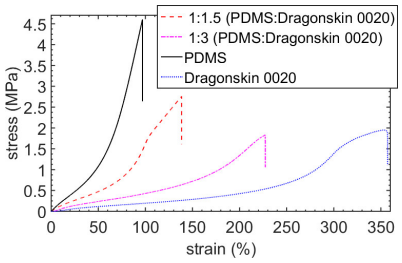

Fig. 2. Stress-strain tests of PDMS, Dragonskin 0020, PDMS- Dragonskin 0020 1:1.5, PDMS- Dragonskin 0020 1:3, Dragonskin 0020.

been proposed in [20] [21]. However, fine control and sensor integration on fully soft systems present several challenges which currently limit their potential in microsurgical applications and the achievable forces with such actuators are limited to the mN range [22]. Introducing rigid structures into soft robots can potentially lead to several advantages, e.g. they could constrain motions in desired directions, thus increasing controllability and reliability of the system. Potential limitations include the range of motion and loosing the capability to squeeze through entrances smaller than its nominal size (unless the rigid structure provides predefined folding patterns). A similar approach has been introduced in [23] and [24], where inflatable pouches have been exploited to actuate origami-inspired mechanisms or in self-folding mechanisms including onboard sensing [25].

In this paper, we integrate soft elastomeric materials in the Pop-up book MEMS process to create multilayer rigid-flex laminates and soft fluidic micro-actuators to demonstrate the possibility of developing simple sensors and actuators at millimeter scales. Finally, based on the results obtained from the characterization of the micro-actuators developed, we assemble multiple actuators into a multi-articulated robotic arm (Fig. 1). The idea is that such an arm could provide additional dexterity and manipulation capabilities during endoscopic procedures if integrated on the tip of the endoscope (Fig. 1). In this paper we are not focused on the design of a specific articulation system, but on how the proposed technology could enable the design of such tools.

II. Design and Fabrication

In the following section, the integration of soft materials and soft fluidic micro-actuators into the Pop-up Book MEMS fabrication process is discussed. The benefits of this approach include providing a soft interface between the mechanisms and the tissue, smoothing of sharp edges resulting from the lamination process, and to exploit soft fluidic actuation in order to build instruments that could safely interact with soft tissue. Furthermore, integrating soft actuators inside a kinematically constrained structure can potentially improve actuation reliability and predictability (relative to fully soft mechanisms). Three example mechanisms are proposed: two bending actuators and one linear actuator with proprioceptive capacitive sensing. To pursue this approach, two technical challenges need to be solved: realizing soft fluidic micro-actuators that can withstand high deformations and bonding the soft material to the rigid laminates.

A. Fabrication of soft fluidic micro-actuators

The soft fluidic micro-actuators are fabricated using soft lithography. This technique typically exploits polydimethylsiloxane (PDMS) that is spun onto silicon molds and thermally cross-linked, thus resulting in layers that can be adhered and sealed irreversibly via oxygen plasma treatment [26]. In order to increase the resistance of PDMS to deformation under pressure that is necessary to actuate pop-up based mechanisms, we mix PDMS (Sylgard 184, MI, USA) with Dragonskin 0020 (Smooth-On, PA, USA). In this way, we obtain a material that still allows fabrication of micrometer-scale feature sizes and at the same time withstands large deformations. Layers of different mass ratios of PDMS and Dragonskin 0020 can then be bonded together via oxygen plasma treatment to build actuators capable of directional deformation. In particular, we fabricate stiffer layers using a 1:1.5 mass ratio (PDMS:Dragonskin 0020) in combination with softer layers using a 1:3 mass ratio (PDMS:Dragonskin 0020). Stress-strain tests of these soft composites, performed according to ISO 37:2005(E), are reported in Fig. 2 along with stress-strain tests of PDMS and Dragonskin 0020 alone. The mass ratio 1:3 is the maximum amount of Dragonskin 0020 that can be added to the polymeric mixture while preserving the capability of sealing layers via oxygen plasma. The effect of adding Dragonskin 0020 to the mixture is to increase the strength to failure and decrease the stiffness as evident in Fig. 2.

The fabrication process of the soft fluidic micro-actuators is illustrated in Fig. 3. We mix PDMS and Dragonskin 0020 using a 1:3 ratio and spin coat the mixture onto a silicon wafer patterned (height of features is approximately 80 μm) with SU-8 photoresist (MicroChem Corp., MA, USA) at 270 rpm for 60 s (resulting in a 0.25 mm thick membrane). The patterned layer is thermally cross-linked for 30 minutes, peeled from the wafer and bonded via oxygen plasma treatment on an unpatterned layer made using a 1:1.5 ratio which is spun at 150rpm for 60s (0.6 mm thick). The micro structures are then cut and bonded irreversibly via oxygen plasma treatment to a hard material (laser machined metal and/or plastic) whose surface is previously functionalized, i.e. activated by oxygen plasma followed by (3-Aminopropyl)triethoxysilane (APTES, Sigma-Aldrich Corp., MO, USA) modification (Fig. 3b) [27]. Through this approach, we obtain an irreversible bond at the interface between soft and hard material without the need for using additional adhesives. The resulting composite material can easily be integrated in the Pop-up Book MEMS fabrication process, realigned with the other laser machined rigid-flex laminates to be bonded in a heated press with Dupont FR0100 sheet adhesive (spacer materials can be inserted to match the height of the soft layer and to help better distribute the pressure on the adhesive during curing), as shown in Fig. 3c. The resulting laminate is laser machined to release the final mechanisms, tubes with I.D. of 254 μm (Micro-Renathane Catheter Tubing, Braintree Scientific, Inc., MA,

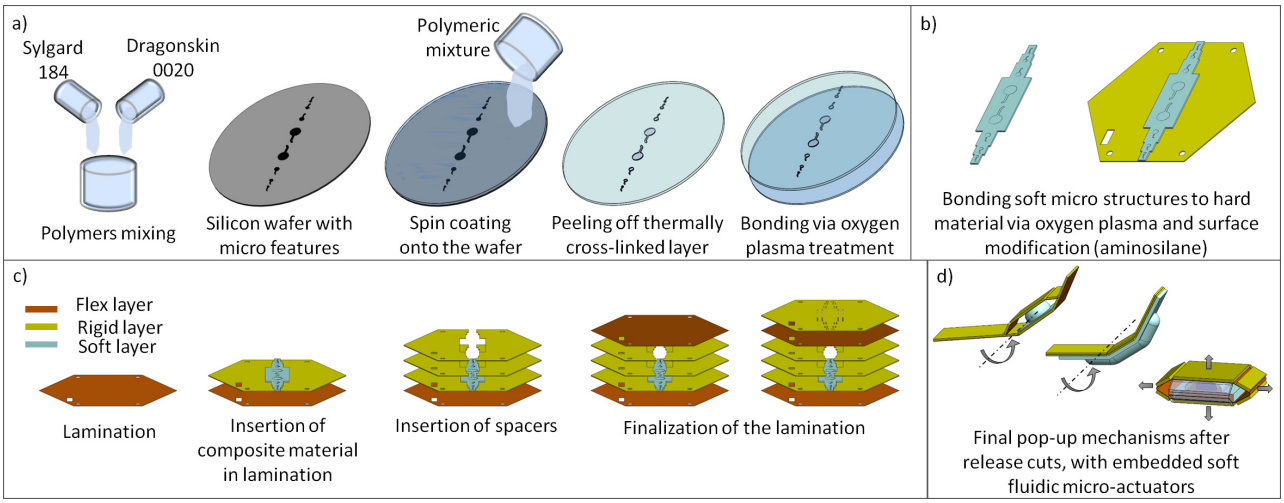

Fig. 3. Schematic of the fabrication and integration process for soft fluidic micro-actuators. a) Fabrication of the actuators via SU-8 patterned silicon wafer. b) Fabrication of a composite layer by bonding the soft patterned layer onto a hard material modified by silanization. c) Integration of the composite layer in the lamination process. d) Final release of the mechanisms and soft fluidic actuation.

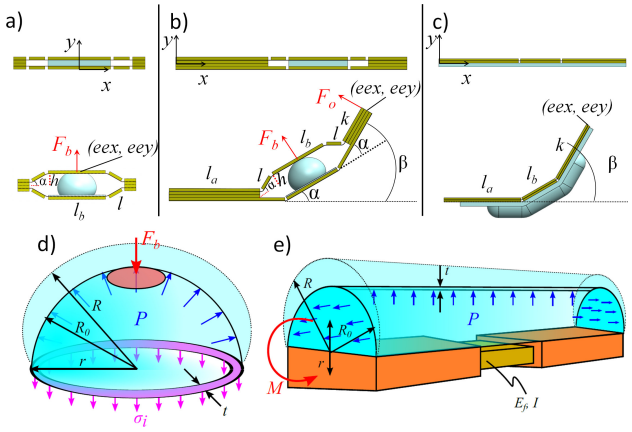

Fig. 4. Illustration of the three proposed soft pop-up mechanisms. a) Linear actuator based on a Sarrus linkage mechanism integrating a soft fluidic micro-actuator in the center. b) Bending mechanism based on the same Sarrus linkage mechanism of a). c) Second bending mechanism based on a series of rigid links with an external soft fluidic micro-actuator. d) Schematic of the model used to describe (a) and (b). e) Schematic of the model used to describe (c).

USA) are inserted and sealed (Poxy Pak, Loctite, USA) and the soft fluidic micro-actuators are pressurized to pop-up and expand the folded mechanisms and provide actuation (Fig. 3d).

B. Design of soft pop-up micro-mechanisms

A linear actuator that could be used for expansion/stabilization mechanisms and injection tasks, as well as bending actuators, which could be exploited for surgical tasks such as tissue retraction and cutting or steering an endoscopic instrument, are presented in the following section. The linear actuator (Fig. 4a) is based on a Sarrus linkage mechanism with an embedded soft micro actuator. The first bending actuator is based on the same Sarrus linkage mechanism, but in this case the two bottom side plates are fixed to convert axial deformation of the inner actuator into bending motion (Fig. 4b), thus we will refer to this mechanism as internal micro-balloon joint (IMJ). The second bending actuator (Fig. 4c) consists of a series of linkages actuated by an external soft balloon, thus we will refer to it as external micro-balloon joint (EMJ). The mechanisms are made of: 254μm glass-reinforced epoxy laminate sheets (garolite) as structural material, 25μm Dupont FR0100 sheet as adhesive and 25μm polyimide film as flexure layers. For the linear actuator, DuPont Pyralux copper/polyimide (18μm copper and 25μm polyimide) is patterned to have conductive inner electrodes on the top and bottom, thus forming a capacitive sensor. The kinematics of the linear actuator can be described by the following geometric model:

$$\begin{bmatrix} eex \\ eey \end{bmatrix} = \begin{bmatrix} 0 \\ 2l\sin\alpha \end{bmatrix} \tag{1}$$

where *eex* and *eey* represent the coordinates of the end effector in Fig. 4a.

To equate the input pressure to deformation of the actuators we first use Laplace's law for a thin-walled sphere (Fig. 4d), we can obtain:

$$F_b = P2\pi R^2 - 2\pi rtE\left(\frac{\Delta R}{R_0}\right) \tag{2}$$

where P is the pressure inside the balloon, E is the elastic modulus of the material (experimentally derived by material characterization, see Fig. 2), r is the balloon diameter when not inflated, t is the thickness of the balloon membrane and R is the total deformation of the micro-balloon in the axial direction (that equals $2h$ in Fig. 4a). In addition we have substituted σ (Fig. 4d) as

$$\sigma = E\frac{\Delta R}{R_0} \tag{3}$$

Therefore the force is directly related to pressure and balloon expansion. We can then relate the balloon expansion to the pressure by applying membrane theory for a circular plate:

$$h = \left(\frac{Pr^4}{128\left(\frac{Et^3}{12(1-\nu^2)}\right)} \right) \tag{4}$$

where ν is the Poisson's ratio of the polymeric material.

Dimensions of the fabricated prototype are: l_b = 3 mm, total thickness = 1.157 mm (including a 0.85 mm thick soft actuator composed of 0.25 mm for the layer of 1:3 PDMS:Dragonskin 0020 ratio and 0.6 mm for the layer of 1:1.5 ratio), and the soft actuator diameter when not inflated is 2.5 mm.

For the IMJ, the total bending range β is:

$$\beta = 2\sin^{-1}(h/l) \tag{5}$$

where h is half of the micro balloon expansion and l is the length of the lateral plate of the Sarrus linkage. For this actuator, four prototypes are fabricated at different dimensions (reported in Tab. I) to evaluate scaling effects: l_b (central plate) and l (lateral plate) are shown in Fig. 4b, and ϕ is the diameter of the non inflated balloon. For each of the prototypes, the total thickness of the laminate is 1.167 mm, the height of the soft actuator when not inflated is 0.8 mm (0.25 mm for the layer of 1:3 PDMS:Dragonskin 0020 ratio and 0.55 mm for the layer of 1:1.5 ratio). For this mechanism, the force exerted by the micro-balloon on the central plate F_b can be geometrically related to the output force generated at the tip of the system F_o:

$$F_o = F_b \left(\frac{l}{l+k} \right) \cos\alpha \tag{6}$$

where α and k are shown in Fig. 4b and F_b is the same as for the linear actuator. The equation describing the trajectory of the end effector (*eex*, *eey*) is reported for the structure in Fig. 4b as a function of design parameters as follows:

$$\begin{bmatrix} eex \\ eey \end{bmatrix} = \begin{bmatrix} l_a + l + cos\alpha(l_b + \sin\alpha(l+k)) \\ \sin\alpha(l_b + \cos\alpha(l+k)) \end{bmatrix} \tag{7}$$

Four prototypes are fabricated at different dimensions for the EMJ as well. Dimensions are reported in Tab. I): l_b (central plate) and the length and width of the non inflated balloon. For each of the prototypes, the total thickness of the rigid laminate is 0.575 mm, the thickness of the soft actuator is 1.15 mm (0.45 mm for the layer of 1:3 PDMS:Dragonskin 0020 ratio and 0.7 mm for the layer of 1:1.5 ratio). We can relate the total bending β of this mechanism and the torque generated M to the input pressure by using the Law of Laplace and modeling the polyimide flexure as a beam (see Fig. 4e):

TABLE I

DIMENSIONS OF THE FABRICATED IMJ AND EMJ PROTOTYPES.

IMJ	l_b (mm)	l (mm)	ϕ (mm)
	5	1.34	3
	2.5	0.55	1.3
	1.75	0.5	0.85
	1	0.324	0.53
EMJ	l_b (mm)	balloon length (mm)	balloon width (mm)
	5	19	3
	2.5	10.45	1
	1.75	7	0.9
	1	6	0.8

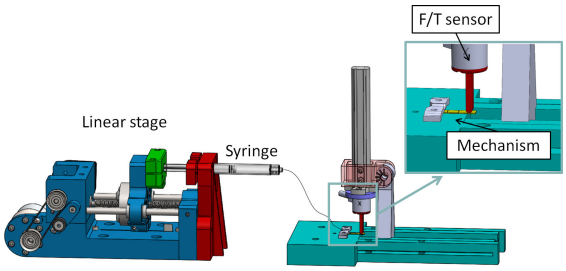

Fig. 5. Evaluation platform for testing the soft pop-up mechanisms composed of a linear stage actuating a 3ml syringe (left), and a frame for fixing the different test mechanisms (right). The configuration shown includes the F/T sensor positioned in contact with the mechanisms (inset). In the case of the bending tests the F/T sensor is removed.

$$P = \frac{Et}{2R}\left(\frac{\Delta R}{R_0}\right) \tag{8}$$

$$M = 2\pi R^2 Pr \tag{9}$$

$$\beta = -\left(\frac{M}{E_f I}\right) \tag{10}$$

where E_f is the elastic modulus of polyimide.

C. Design of a soft pop-up multi-articulated robotic arm

Based on the design of the soft pop-up mechanisms presented in Fig. 4, a simple system integrating multiple degrees of freedom (DOFs) is designed. The structure, integrated at the tip of an endoscope (Fig. 1), is composed of: a four-bar linkage mechanism for expansion, thus allowing surgical triangulation, a yaw DOF (based on the design of Fig. 4c) and a pitch DOF (based on the mechanism of Fig. 4b) to steer the end effector and perform tissue manipulation. The first two mechanisms are 5 mm wide, while the third is 2.5 mm. The total length is 35 mm, coming out of the tip of the endoscope by 12 mm. The thickness of the structure is equal to one of the single mechanisms. Such a structure is presented as a demonstration of how to integrate the multiple elements described in this paper and as a proof of concept that we can design articulated medical instruments exploiting the proposed soft pop-up technology.

III. EXPERIMENTS

The linear actuator is characterized in terms of capacitance variation as a function of the distance between the plates. The two bending actuators are experimentally characterized to determine the maximum torque generated in isostatic conditions and the maximum free bending angle. An evaluation platform is designed and fabricated in order to test the mechanisms (Fig. 5). The platform consists of a linear

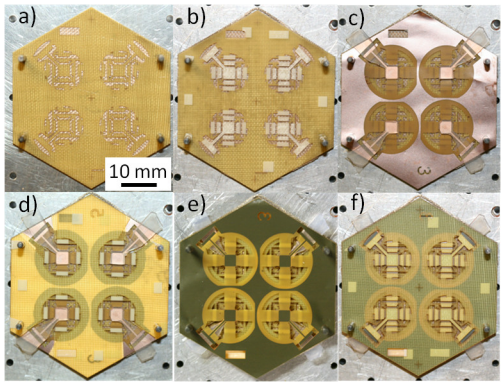

Fig. 6. Fabrication process of the soft pop-up linear actuator with proprioceptive sensing. a) Rigid laminates are aligned using precision dowel pins. b) 25 m Dupont FR0100 sheet adhesive is applied. c) The composite layer of soft and rigid material is integrated. d) Spacers are inserted. e)-f) The lamination continues until the all the necessary layers are inserted.

stage actuating a syringe 1 mm/s corresponding to a water flow of 0.01 ml/s. Pressure, force and capacitance data are acquired using a NI USB-6002 board and data collection is performed in LabVIEW (National Instruments, Austin, TX, USA).

A. Capacitance variation characterization

Capacitance variation versus increasing distance between the conductive plates is measured by applying increasing pressures through the same setup and measuring the capacitance through an AD7746 evaluation board (Analog Devices, Norwood, MA, USA) with the following specifications: resolution 4aF, accuracy 4fF, update rate 50Hz.

B. Torque characterization

Torque characterization is performed by placing the joints in a straight configuration (0° bending), constraining one side and placing the other in contact with a F/T sensor (Nano 17, ATI Industrial Automation NC, USA), as shown in the inset of Fig. 5. Torque is computed by multiplying the measured force by the moment arm (i.e. the distance between the center of the central plate and the point of contact with the F/T sensor). Tests are repeated three times for each joint and two joints of each size are tested. The IMJ is tested for pressures up to 500 kPa, while the EMJ up to 200 kPa. The pressure limits are chosen to minimize the risk of failure. Pressures in the same range have already been tested in devices for MIS [28] safely. Pressure is recorded using a pressure sensor (BSP B010-EV002-A00A0B-S4, Balluff, USA), not shown in Fig. 5.

C. Bending characterization

The bending characterization is performed applying increasing pressure in the joints and resolving the correspondent bending angle visually. Images are taken by placing a camera on a tripod parallel to the joint and analyzed in Matlab (Mathworks Inc., Natick, MA, USA). The IMJ is tested for pressures up to 350 kPa, while the EMJ up to 200 kPa. Also in this case pressures are chosen in order to safely and repeatedly test the samples with low risk of failure or leakages.

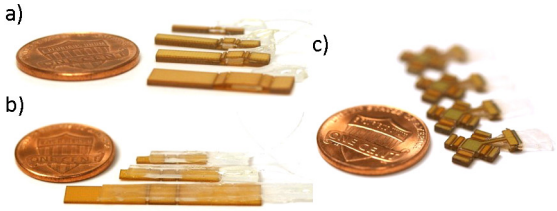

Fig. 7. Fully functional fabricated prototypes based on the soft pop-up approach: a) IMJ at different scales, b) EMJ at different scales, c) linear actuator with capacitive proprioceptive sensing.

D. Multi-articulated robotic arm demonstration

The multi-articulated robotic arm is mounted on top of an endoscope model (10mm diameter tube) to demonstrate the capability of performing simple potential surgical tasks: expanding the mechanism to perform triangulation, yaw DOF to steer the end effector and pitch DOF to approach tissue.

IV. Results and Discussion

Fully functional prototypes have been fabricated and tested. Since each of the mechanisms follow the same fabrication process (Fig. 3), only the fabrication steps for the linear actuator are presented in Fig. 6. Each of the fabricated prototypes based on the proposed soft pop-up technology, are shown in Fig. 7.

A. Capacitance variation characterization

The capacitance measured during actuation of the linear actuator is reported in Fig. 8. The capacitance is normalized in order to more easily compare different prototypes. A maximum capacitance variation of 0.21 pF is observed with a linear actuation of up to 1.45 mm. Please refer to the attached video for a demo capacitance variations during actuation of this system.

B. Torque characterization

Torque characterization results are reported in Fig. 9 and Fig. 10 respectively for the IMJ and the EMJ. On the same plots the results from the analytical model described in

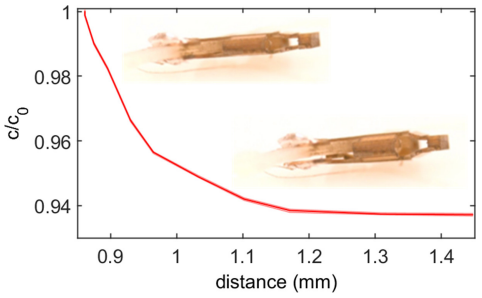

Fig. 8. Results of the capacitance characterization during actuation of the linear actuator. Solid line is the mean value and shaded area represents one standard deviation computed on two prototypes, tested three times each. The top left inset shows the unactuated prototype (maximum value of capacitance), the bottom right inset shows the actuated prototype.

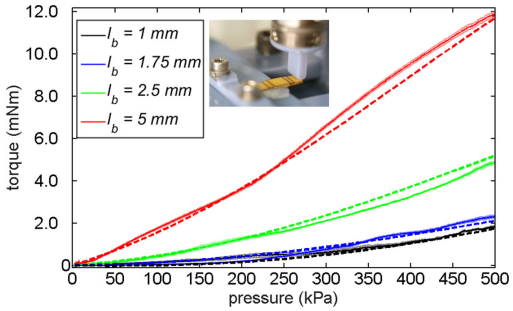

Fig. 9. Results of the torque characterization test for the IMJ prototypes fabricated at different scales (l_b). The dashed lines represent the output from the model. The picture in the inset shows the actuator during the test. Solid line is the mean value and the shaded area represents one standard deviation computed on two prototypes for each size, tested three times each.

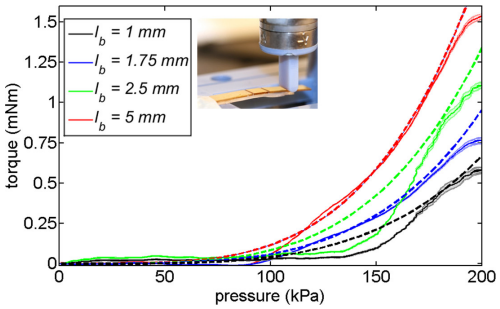

Fig. 10. Results of the torque characterization test for the EMJ prototypes fabricated at different scales (l_b). The dashed lines represent the output from the model. The picture in the inset shows the actuator during the test. Solid line is the mean value and the shaded area represents one standard deviation computed on two prototypes for each size, tested three times each.

section II.B are shown. The model is able to predict the experimental data quite accurately both for the IMJ and the EMJ. In the case of the EMJ the model tends to overestimate at higher pressures most likely because in that case the balloon tends to expand more radially than axially, thus contributing less to the torque. The numerical values from the experiments are reported in Tab. II. The IMJ is able to generate maximum torques ranging from 1.841±0.07 mNm to 11.87±0.12 mNm, depending on the size of the prototype. Depending on the arm length, relatively high forces can be obtained with the IMJ, for example with the largest prototype, a force of 2.4 N can be generated with a 5 mm arm and with the smallest prototype a force of 0.5N can be obtained with a 3.5 mm arm. In addition, it is worth noting that the IMJ can be tested up to 500kPa, since the balloon is constrained not to expand by the surrounding pop-up mechanism and thus the risk of failure due to large deformation of the soft actuator is reduced. In the case of the EMJ, the balloon tends to expand in the direction of lower impedance (opposite direction with respect to the load cell) and thus it is not able to safely reach the same pressure. The EMJ provides lower torques, between 1.5 and 0.6 mNm, resulting in forces on the order of hundreds of milliNewtons. In addition, they start applying measurable forces on the F/T sensor after a pressure of 100kPa is applied, since before that pressure the fluid introduced is mainly inflating the balloon in the lower impedance direction (where it is not constrained by any surrounding pop-up mechanism).

C. Bending characterization

Bending angle characterization results are reported in Fig. 11 and Fig. 12 respectively for the IMJ and the EMJ. The model is able to follow the trend of the experimental data quite accurately, although it tends to overestimate the bending at lower pressures, likely due to the hyperelastic behavior of the elastomer, which is approximated as linear in the model. In the case of the larger joint, the model tends to overestimate the bending, probably because the balloon starts being more significantly bent and thus the spherical approximation starts to fail. On the other hand, in the case of the EMJ the model is not able to fully get the trend of the experimental data. This is mainly due to lower accuracy in the integration of the actuator during fabrication (not perfectly centered or aligned in some cases). In addition, the proposed model neglects the pressures acting in the radial direction (perpendicular to the plates of the EMJ). Despite this, the model can be exploited as a first order approximation of the system in the design process. Numerical values of the maximum bending angles of the different actuators are summarized in Tab. II. In this case, the design of the EMJ provides higher bending capabilities, reaching almost 90°. The IMJ also provides large bending, around 60°. What seems to limit the bending capabilities of this design is that at higher pressure, the surrounding pop-up mechanism starts offering increasing resistance to the balloon expansion, which starts expanding laterally (pushing on the lateral plates) instead of axially. The current design controls bending by pressurizing the soft actuators with water and decreasing the bending angle by removing the water. The restoring motion relies mainly on the strain energy stored in the elastomer as well as on the incompressibility of water. The bending results are also shown in the attached video for the IMJ and EMJ (2.5 mm).

D. Multi-articulated robotic arm demonstration

Fig. 13 shows the multi-articulated robotic arm based on soft fluidic micro-actuators and pop-up mechanisms while

TABLE II

TORQUE AND BENDING CHARACTERIZATION RESULTS. FORCES ARE COMPUTED CONSIDERING THE ARM AS HALF OF THE CENTRAL PLATE (l_b) PLUS 2.5 MM (k IN FIG. 4).

	l_b (mm)	Max torque (mNm)	Force (N) @k=2.5mm	Max bending angle (°)
IMJ				
	5	11.9±0.1	2.4	66.3±1.4
	2.5	4.9±0.1	1.3	73.8±1.6
	1.75	2.3±0.1	0.68	42.6±1.6
	1	1.8±0.1	0.5	21.1±1.2
EMJ				
	5	1.53±0.02	0.3	89.4±2.1
	2.5	1.11±0.03	0.2	77.8±0.9
	1.75	0.77±0.03	0.4	89.0±2.4
	1	0.58±0.02	0.2	55.7±1.2

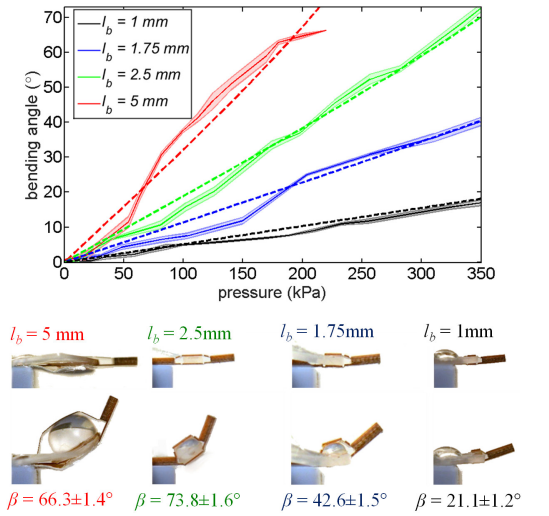

Fig. 11. Results of the bending angle characterization test for the IMJ prototypes fabricated at different scales (l_b). The dashed line represents the output from the model. The pictures on the bottom show the prototypes at different l_b dimensions at minimum and maximum bending angle. Solid line is the mean value and the shaded area represents one standard deviation computed on two prototypes for each size, tested three times each.

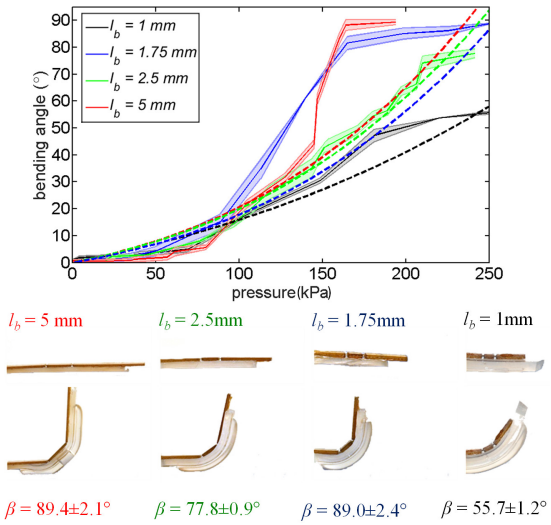

Fig. 12. Results of the bending angle characterization test for the EMJ prototypes fabricated at different scales (l_b). The dashed line represents the output from the model. The pictures on the bottom show all the prototypes at different l_b at minimum and maximum bending angle. Solid line is the mean value and the shaded area represents one standard deviation computed on two prototypes for each size, tested three times each.

demonstrating potential surgical tasks mounted on top of an endoscope model (10 mm diameter plastic tube). Expansion is obtained by inflating the balloon circled in Fig. 13b, which causes the four-bar linkage to open. Yaw is obtained with the EMJ (that provides larger bending) (Fig. 13c): the actuator is mounted in such a way that it provides structural stiffness in the direction where the tissue is pulled. For the pitch DOF the IMJ is exploited (higher force) (Fig. 13d). The IMJ is designed for unidirectional bending, thus avoiding undesired motions during tissue pulling. This last DOF could potentially be used to perform tissue retraction tasks, if

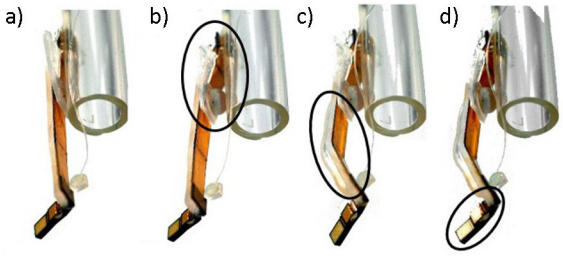

Fig. 13. Multi-articulated robotic arm. a)-b) Expansion of the soft pop-up parallel mechanism to perform triangulation. c) Yaw DOF, d) pitch DOF.

provided with an appropriate end effector. In the attached video the multi-articulated robotic arm demonstrates the capability of expanding the mechanism, and performing yaw and pitch motions.

V. CONCLUSIONS

In this paper, we introduce a manufacturing technique for integrating soft materials and soft fluidic micro-actuators into the pop-up book MEMS fabrication process. Different mechanisms are proposed for sensors and actuators at scales ranging from 5 mm down to 1 mm, showing the robustness of the proposed method in scaling the design. The fabrication process is low cost and allows batch manufacturing. The soft materials are designed in order to provide the desired properties both from a chemical and mechanical point of view, thus enabling the possibility to exploit soft lithography and oxygen plasma treatment to obtain features on the micrometer scale and large deformations. The proposed soft pop-up approach allows flexibility in the material selection, thus different materials can be integrated according to specific application requirements (e.g. biocompatibility). All materials used have been previously applied in disposable medical devices: in particular, polyimide, garolite and PDMS are biocompatible. Additional biocompatible materials could be used (e.g. AISI 316l stainless steel, titanium, different adhesives and elastomers) and integrating these materials is the subject of future work. Each actuator has been fabricated and tested experimentally in terms of bending capabilities and forces generated. All prototypes were functional and did not exhibit leaking even after repetitive testing up to 500 life cycles. Two different integration strategies have been demonstrated: with regards to the design of the IMJ, we constrain the axial deformation of the micro balloon to actuate a Sarrus linkage mechanism (by bonding the micro balloon internally), while in the design of the EMJ we bond the micro balloon externally with respect to the rigid laminate. The first strategy leads to high forces and moderate bending angles, while the second results in large bending angles and low forces. In general, the pop-up structure successfully constrains the kinematics of the mechanisms during the actuation of the soft micro balloons. We provided analytic tools for guiding the design process and we validated them with the experimental data. According to these models, future design optimization will be performed to minimize the balloon deformation during bending. Also, additional

testing will be performed, including stiffness characterization for backdrivability. The proposed fabrication process enables integration of sensing capabilities: a proof of concept of monitoring capacitance variation during actuation is successfully demonstrated and we plan to further investigate the possibility of closed-loop control of the mechanisms using this embedded sensing. The presented mechanisms demonstrated forces and dexterity that make them suitable candidates for designing novel micro surgical tools. Indeed, forces required in endoscopic procedures are typically below 1 N for endoluminal retraction tasks (tensioning the tissue for easing the cutting procedure) [9]. The possibility of easily scaling down the mechanisms makes the technology promising for procedures which are currently difficult to perform in a minimally invasive way, such as interventional bronchoscopy. The minimum tested operational frequency (to inflate the larger balloons) is 14 Hz with a flow rate of 0.01 ml/s in a 254 μm diameter pipe running along a 1 m long endoscope. Typical frequency range during microsurgical tasks is 0-1.7 Hz [29]. Finally, the presented systems are integrated to fabricate a demonstration piece of a multi-articulated robotic arm that is mounted on top of an endoscope model to demonstrate simple tasks that could be useful in a surgical scenario such as: expansion of the mechanism to perform triangulation, yaw and pitch to steer the end effector and approach tissue.

ACKNOWLEDGMENT

The authors would like to acknowledge the Wyss Institute for Biologically-Inspired Engineering for their support of this work. The authors would also like to acknowledge DARPA (grant FA8650-15-C-7548).

REFERENCES

[1] C. Bergeles and G.-Z. Yang, "From passive tool holders to microsurgeons: safer, smaller, smarter surgical robots," *Biomedical Engineering, IEEE Transactions on*, vol. 61, no. 5, pp. 1565–1576, 2014.

[2] A. Loeve, P. Breedveld, and J. Dankelman, "Scopes too flexible... and too stiff," *IEEE pulse*, vol. 1, no. 3, pp. 26–41, 2010.

[3] V. Vitiello, S.-L. Lee, T. P. Cundy, and G.-Z. Yang, "Emerging robotic platforms for minimally invasive surgery," *Biomedical Engineering, IEEE Reviews in*, vol. 6, pp. 111–126, 2013.

[4] B. P. M. Yeung and T. Gourlay, "A technical review of flexible endoscopic multitasking platforms," *International Journal of Surgery*, vol. 10, no. 7, pp. 345 – 354, 2012. [Online]. Available: http://www.sciencedirect.com/science/article/pii/S1743919112001069

[5] S. J. Phee, S. C. Low, V. Huynh, A. P. Kencana, Z. Sun, and K. Yang, "Master and slave transluminal endoscopic robot (master) for natural orifice transluminal endoscopic surgery (notes)," in *Engineering in Medicine and Biology Society, 2009. EMBC 2009. Annual International Conference of the IEEE*. IEEE, 2009, pp. 1192–1195.

[6] A. Arezzo, T. Ranzani, A. Menciassi, M. Bonino, M. Morino, and P. Dario, "Endoscopio red," Italy Patent FI2013A000055, 2015.

[7] G. P. Mylonas, V. Vitiello, T. P. Cundy, A. Darzi, and G.-Z. Yang, "Cyclops: A versatile robotic tool for bimanual single-access and natural-orifice endoscopic surgery," in *Robotics and Automation (ICRA), 2014 IEEE International Conference on*. IEEE, 2014, pp. 2436–2442.

[8] S. Russo, P. Dario, and A. Menciassi, "A novel robotic platform for laser-assisted transurethral surgery of the prostate," *Biomedical Engineering, IEEE Transactions on*, vol. 62, no. 2, pp. 489–500, Feb 2015.

[9] T. Ranzani, G. Ciuti, G. Tortora, A. Arezzo, S. Arolfo, M. Morino, and A. Menciassi, "A novel device for measuring forces in endoluminal procedures," *International Journal of Advanced Robotic Systems*, vol. 12, 2015.

[10] R. J. Hendrick, C. R. Mitchell, S. D. Herrell, and R. J. Webster, "Hand-held transendoscopic robotic manipulators: A transurethral laser prostate surgery case study," *The International Journal of Robotics Research*, p. 0278364915585397, 2015.

[11] P. J. Swaney, A. W. Mahoney, A. A. Remirez, E. Lamers, B. I. Hartley, R. H. Feins, R. Alterovitz, and R. J. Webster III, "Tendons, concentric tubes, and a bevel tip: Three steerable robots in one transoral lung access system," in *Robotics and Automation (ICRA), 2015 IEEE International Conference on*. IEEE, 2015, pp. 5378–5383.

[12] S. C. Ryu and P. E. Dupont, "Fbg-based shape sensing tubes for continuum robots," in *Robotics and Automation (ICRA), 2014 IEEE International Conference on*. IEEE, 2014, pp. 3531–3537.

[13] J. Whitney, P. Sreetharan, K. Ma, and R. Wood, "Pop-up book mems," *Journal of Micromechanics and Microengineering*, vol. 21, no. 11, p. 115021, 2011.

[14] K. Y. Ma, P. Chirarattananon, S. B. Fuller, and R. J. Wood, "Controlled flight of a biologically inspired, insect-scale robot," *Science*, vol. 340, no. 6132, pp. 603–607, 2013.

[15] J. B. Gafford, S. B. Kesner, R. J. Wood, and C. J. Walsh, "Force-sensing surgical grasper enabled by pop-up book mems," in *Intelligent Robots and Systems (IROS), 2013 IEEE/RSJ International Conference on*. IEEE, 2013, pp. 2552–2558.

[16] J. Gafford, S. Kesner, A. Degirmenci, R. Wood, R. Howe, and C. Walsh, "A monolithic approach to fabricating low-cost, millimeter-scale multi-axis force sensors for minimally-invasive surgery," in *Robotics and Automation (ICRA), 2014 IEEE International Conference on*, May 2014, pp. 1419–1425.

[17] J. Gafford, R. Wood, and C. Walsh, "Self-assembling, low-cost, and modular mm-scale force sensor," *Sensors Journal, IEEE*, vol. 16, no. 1, pp. 69–76, Jan 2016.

[18] M. Cianchetti, T. Ranzani, G. Gerboni, T. Nanayakkara, K. Althoefer, P. Dasgupta, and A. Menciassi, "Soft robotics technologies to address shortcomings in today's minimally invasive surgery: The stiff-flop approach," *Soft Robotic*, vol. 1, no. 2, pp. 122–131, June 2014. [Online]. Available: http://online.liebertpub.com/doi/pdf/10.1089/soro.2014.0001

[19] T. Ranzani, G. Gerboni, M. Cianchetti, and A. Menciassi, "A bioinspired soft manipulator for minimally invasive surgery," *Bioinspiration & Biomimetics*, vol. 10, no. 3, p. 035008, 2015. [Online]. Available: http://stacks.iop.org/1748-3190/10/i=3/a=035008

[20] K. Ikuta, H. Ichikawa, K. Suzuki, and T. Yamamoto, "Safety active catheter with multi-segments driven by innovative hydro-pressure micro actuators," in *Micro Electro Mechanical Systems, 2003. MEMS-03 Kyoto. IEEE The Sixteenth Annual International Conference on*, Jan 2003, pp. 130–135.

[21] S. Konishi, "Small soft safe micromachines for biomedical applications," in *Electron Devices Meeting (IEDM), 2014 IEEE International*, Dec 2014, pp. 31.6.1–31.6.4.

[22] B. Gorissen, M. De Volder, A. De Greef, and D. Reynaerts, "Theoretical and experimental analysis of pneumatic balloon microactuators," *Sensors and Actuators A: Physical*, vol. 168, no. 1, pp. 58–65, 2011.

[23] R. Niiyama, D. Rus, and S. Kim, "Pouch motors: Printable/inflatable soft actuators for robotics," in *Robotics and Automation (ICRA), 2014 IEEE International Conference on*, May 2014, pp. 6332–6337.

[24] S. Yim and S. Kim, "Origami-inspired printable tele-micromanipulation system," in *Robotics and Automation (ICRA), 2015 IEEE International Conference on*, May 2015, pp. 2704–2709.

[25] X. Sun, S. Felton, R. Wood, and S. Kim, "Printing angle sensors for foldable robots," in *Intelligent Robots and Systems (IROS), 2015 IEEE/RSJ International Conference on*, Sept 2015, pp. 1725–1731.

[26] D. Qin, Y. Xia, and G. M. Whitesides, "Soft lithography for micro-and nanoscale patterning," *Nature protocols*, vol. 5, no. 3, pp. 491–502, 2010.

[27] V. Sunkara, D.-K. Park, and Y.-K. Cho, "Versatile method for bonding hard and soft materials," *Rsc Advances*, vol. 2, no. 24, pp. 9066–9070, 2012.

[28] A. Moers, M. De Volder, and D. Reynaerts, "Integrated high pressure microhydraulic actuation and control for surgical instruments," *Biomedical microdevices*, vol. 14, no. 4, pp. 699–708, 2012.

[29] F. Hammond, S. Talbot, R. Wood, and R. Howe, "Data-driven design of a dexterous robotic microsurgery system," in *Design of Medical Devices Conf., Minneapolis, MN*, 2012.